Real-Time Tendon Strain Estimation of Rotator-Cuff Muscles during Robotic-Assisted Rehabilitation

Beck, I.L.Y.; Belli, I.; Peternel, L.; Seth, A.; Prendergast, J.M.

DOI
10.1109/Humanoids57100.2023.10375158

Publication date
2023

Document Version
Final published version

Published in
Proceedings of the 2023 IEEE-RAS 22nd International Conference on Humanoid Robots (Humanoids)

Real-Time Tendon Strain Estimation of Rotator-Cuff Muscles during Robotic-Assisted Rehabilitation

Irene Beck[1], Italo Belli[1,2], Luka Peternel[1], Ajay Seth[2] and J. Micah Prendergast[1,*]

2023 IEEE-RAS 22nd International Conference on Humanoid Robots (Humanoids) | 979-8-3503-0327-8/23/$31.00 ©2023 IEEE | DOI: 10.1109/HUMANOIDS57100.2023.10375158

***Abstract*— In this research, we propose a novel method to estimate and monitor rotator cuff tendon strains during active robotic-assisted rehabilitation. This is a significant step forward from our previous work which estimated these tendon strains during passive exercises (i.e., no muscle activity). Physiotherapists adopt a cautious approach to rehabilitation treatment to prevent (re-) injury given the limited available information about the shoulder's internal condition. By leveraging a robotic device and a musculoskeletal model, our approach provides quantitative information on the risk of re-injury by monitoring the strains of the rotator cuff tendons during shoulder movements with the application of external loads. Muscle strains depend on the shoulder kinematic state and muscle activations, which makes it crucial to obtain physiologically realistic joint kinematics to estimate real-time muscle function. To obtain the strains, we utilize our muscle redundancy solver that incorporates constraints on model accelerations, the glenohumeral joint reaction forces, and active muscle dynamics. Using this algorithm along with force and pose data from a collaborative robotic arm, we demonstrate the ability to update our tendon strain estimates based on muscle activation during robotic-assisted rehabilitation exercises. The findings of our research pave the way for establishing improved therapy that considers the risk of injury to individual muscles and explores a broader and more personalized range of motion. By providing physiotherapists with valuable quantitative information on rotator cuff tendon strains, our method empowers them to optimize rehabilitation protocols and deliver more personalized and effective care. In addition, the system and method presented here comprise a tool capable of offering new insights into the relationship between the rotator cuff muscles, external forces, and shoulder kinematics.**

I. Introduction

The shoulder complex is one of the most common sites for musculoskeletal disorders [1], with 70% of shoulder complaints attributed to disease or injury to the rotator cuff (RC) muscle-tendon units [2]. Tearing of the rotator cuff tendons results primarily in pain, loss of strength and a restricted range of motion of the upper limb, which may affect the ability to perform work and/or activities of daily living [3]. The likelihood of RC tears also increases with age, with over 50% of people aged 60 or older suffering from one or more RC tears [4], [5]. In addition, repetitive overhead activities during work, or competitive sports also increase the risk of RC tears [6]–[8].

Conventional treatment of RC tears requires intensive rehabilitation via physiotherapy. This rehabilitation may follow surgical repair in the case of severe tears, but is the standard of treatment for all RC injuries. Effective rehabilitation after surgery is necessary to prevent shoulder joint stiffness, regain range of motion and limit the risk of re-tearing [9]. Regardless of the treatment type, RC rehabilitation is time-intensive with significant improvement occurring after twelve weeks [10] and many patients are instructed to continue home exercises for as long as six months to a year [11], [12].

Due to the complexity of the shoulder joint and a lack of quantitative insight into the risks of re-tear, the exercises used in conventional RC rehabilitation are typically highly conservative and comprised of single-degree-of-freedom motions even when assisted by an experienced physiotherapist [13]. It is likely that this limited range of motion during rehabilitation may delay recovery, whereas moving through a larger range of motion could result in expedited recovery [14], [15]. Additionally, current rehabilitation techniques are demanding for physiotherapists who must physically manipulate many patients per day and who are limited to assisting one patient at a time [16]. Finally, treatment of the rotator cuff is often inadequate, leaving patients with persistent symptoms [17], inhibiting the patient's ability to work and perform daily activities in the long term.

Robotic systems can serve to address many of the limitations of conventional physiotherapy — providing a means for physiotherapists to treat more patients and to customize rehabilitation to a patient's specific needs. Several robots and exoskeletons exist for the rehabilitation of the upper limb [18]–[21]. Robotic devices can provide high-intensity, repetitive exercises that target specific injuries/joints [22], [23]. Additionally, a robotic system can leverage its sensing capabilities to measure joint positions, velocities, accelerations, and torques [24] and provide force feedback. These metrics can be monitored objectively and reliably throughout a rehabilitation program to assess the patient's progress [16].

In the case of rehabilitation of RC tears, monitoring the subject's muscle tension is of interest to prevent (re-)tearing of the tendons. The nature of the RC as deeper (below superficial) muscles, combined with the soft-tissue structures of the glenohumeral (GH) joint, makes lab-based motion-capture and electromyography (EMG) measurements impractical for evaluating the function of RC muscles. Musculoskeletal modeling, in combination with robotic measurements, could provide a physiotherapist with quantitative information on the biomechanics of the shoulder complex and RC muscles.

In our previous work, we developed a method to link musculoskeletal modeling to robotic rehabilitation by captur-

Authors are with the Department of Cognitive Robotics[1] and the Department of BioMechanical Engineering[2], Delft University of Technology, Delft, The Netherlands

*Corresponding author (j.m.prendergast@tudelft.nl)

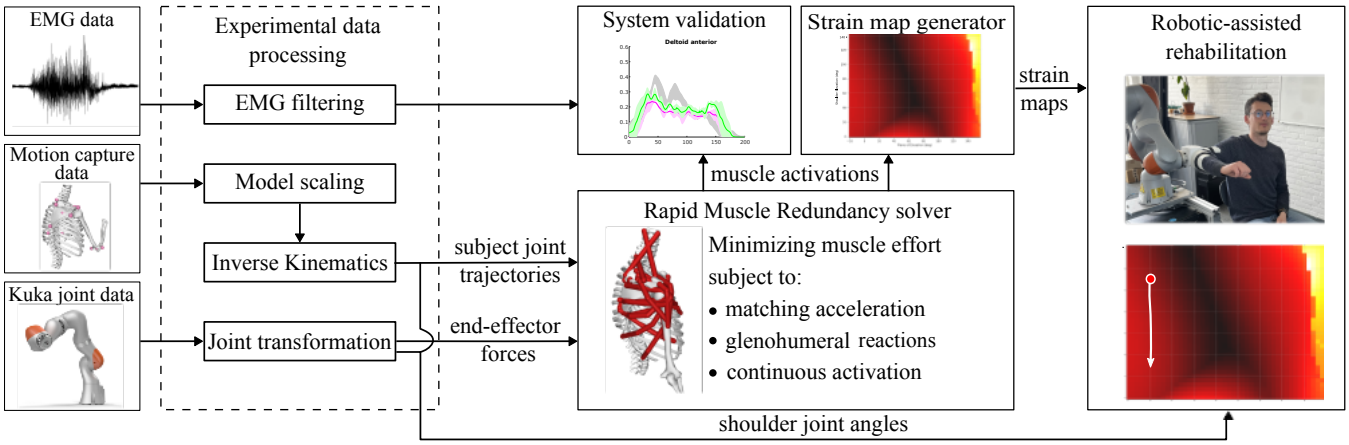

Fig. 1: Workflow for active robotic-assisted shoulder rehabilitation that provides quantitative insights into the risk of re-injury. The experimental data (left) is obtained via motion capture using optical markers or shoulder joint estimates during a human-robot interaction. The experimental data is processed to obtain the joint trajectories and external forces. The Rapid Muscle Redundancy solver (center) is used to estimate muscle activations from a musculoskeletal model for a given (measured) trajectory. The estimated muscle activations are validated against experimental EMG data and used to compute rotator cuff tendon strains. These strains are visualized in "strain maps" (bottom right) and are used to visualize the internal biomechanics of the shoulder during rehabilitation.

ing the relationship between the tendon strains and shoulder state in the form of "strain maps" [25]. These strain maps are an intuitive representation of the RC tendon strains and can be used to minimize the risk of re-injury of the RC tendons while maximizing the range of motion. We recently implemented strain maps to enable a subject to perform robotic-assisted exercises while being protected from potentially dangerous poses [26] in real-time. A major limitation of these maps however, is that they do not incorporate muscle activation into the muscle-tendon strain estimates. This restricts the use of these maps to passive motions (i.e., no external forces) in which the weight of the arm is supported entirely by the robot or a physical therapist and thus limits the use of this tool to early-stage rehabilitation.

To address this limitation, we have developed a novel active strain maps approach that accounts for muscle contributions in various shoulder states (i.e., shoulder joint coordinates and external forces) as sensed by a collaborative robotic manipulator. We exploit our recently developed open-source Rapid Muscle Redundancy (RMR) solver [27] to estimate shoulder muscle activity. The proposed method then transforms these muscle activity estimates into our estimates of tendon strain for all of the RC tendons and creates active strain maps. Finally, we integrate these active strain maps with our robotic physical therapy (PTbot) system using the Kuka LBR iiwa 7 robotic arm. We demonstrate the use of these active maps with the collaborative robot during several conventional shoulder exercises.

II. Methods

The methodology is divided into five subsections. Section II-A gives an overview of the musculoskeletal shoulder model that is leveraged to obtain information on the internal biomechanics of the shoulder during rehabilitation. Section II-B provides a summary of the muscle redundancy problem and how we solve for muscle activations, while

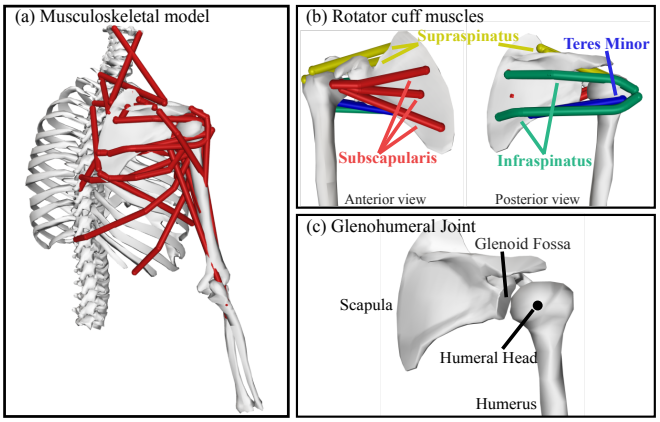

Fig. 2: An overview of the thoracoscapular model. (a) The musculoskeletal shoulder model, and in red, all the actuating muscles. (b) The rotator cuff complex, the four rotator cuff muscles are represented by eight muscle elements; Infraspinatus - green, supraspinatus - yellow, subscapularis - red, teres minor - blue. (c) The glenohumeral joint, detailing the relation between the humeral head and the glenoid fossa of the scapula.

considering active muscle dynamics and the GH joint stability. Section II-C shows the validation of the Python-RMR solver. Section II-D explains how our PTbot system is controlled to provide safe physiotherapy. Section II-E details the experimental design incorporating the active strain maps with the PTbot system. The proposed method is outlined as a block diagram in Figure 1.

A. Musculoskeletal Shoulder Model and Strain Maps

We leveraged the thoracoscapular musculoskeletal shoulder model [28] and the open-source simulation software OpenSim [29] to estimate rotator cuff muscle forces and tendon strains during shoulder exercises. This model, featuring $N_q = 7$ degrees of freedom (DoFs) and actuated by $N_m = 33$ muscle bundles, is designed to provide high fidelity and accurate representation of the shoulder complex by decoupling the movement of the humerus from the scapula. The complete shoulder kinematics are represented by 4 joints:

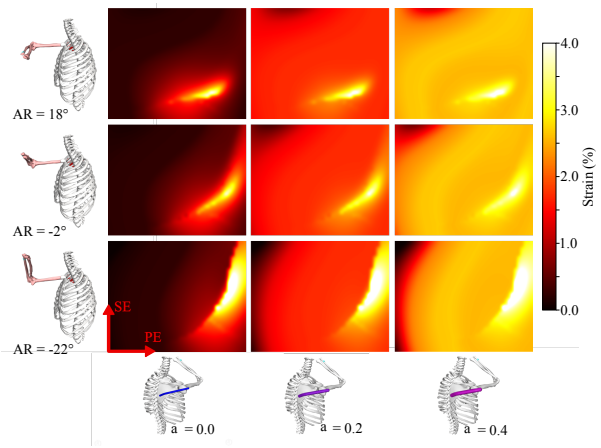

Fig. 3: Interpreting tendon strain from the visualization of strain maps. This example considers the infraspinatus inferior; it includes nine strain maps for a combination of three different axial rotations and three muscle activation levels. The individual maps include the plane of elevation and shoulder elevation on the x- and y-axis, respectively. The columns represent the strain maps for increasing muscle activation a of the infraspinatus inferior (a = 0.0, a = 0.2, and a = 0.4). The rows show strain maps for selected axial rotation angles (AR = -22°, AR = -2°, and AR = 18°).

the scapulothoracic [30], glenohumeral, acromioclavicular, and sternoclavicular joints. Of particular interest in our study are the 4 rotator cuff muscles: infraspinatus, subscapularis, supraspinatus, and teres minor, which span and stabilize the glenohumeral joint. The glenohumeral joint is represented as a three DoFs gimbal joint (Figure 2) and the rotator cuffs primarily affect the direction of the glenohumeral joint reaction force. The strain in the rotator cuff tendons is a measure of (re-)tearing risk [25], [26]. Muscle strains are dependent on the shoulder state and muscle activations, which must be accurately and reliably estimated.

Computing the RC tendon strains from the musculoskeletal model directly is computationally expensive and only provides individual strain values in numerical form, which would be difficult to interpret on its own during rehabilitation. Instead, we chose to enumerate RC muscle strains into a simple yet comprehensive and intuitive view of the possible strain landscape we call "strain map" [25], [26] that enable the physiotherapist to see where they are going in terms of increasing or decreasing strain. Strain maps provide the user with a high-resolution visualization of the tendon strain in the joint space. Different combinations of strains can be utilized depending on the patient's injury and progress during therapy. For example, the strain maps of all rotator cuff muscle elements can be combined into a single strain map by taking the maximum strain for each pose. A strain map may also be visualized for a single muscle (element) to ensure that strains are safe during rehabilitation of a specific injury with a known muscle-tendon location (i.e., a surgical repair of supraspinatus).

Since the rotator cuff muscles only span the GH joint, we consider the 3 shoulder DoFs as the state $\boldsymbol{x}$ of our model, consisting of the following Euler angles; plane of elevation (PE), shoulder elevation (SE), and axial rotation (AR):

$$\boldsymbol{x} = [\ \text{PE},\ \text{SE},\ \text{AR}\ ]\ . \tag{1}$$

The range of shoulder DoFs was constrained within the physiological limits of $-20° \leq PE \leq 160°$, $0° \leq SE \leq 144°$, and $-90° \leq AR \leq 100°$. Rotator cuff tendon strain estimations were pre-computed from the musculoskeletal model for each combination of $\boldsymbol{x}$ at $4°$ intervals and muscle activation in 0.005 activation level intervals.

To visualize the four-dimensional space for a physiotherapist, the strain maps were divided into two-dimensional layers/maps with the plane of elevation and shoulder elevation on the x- and y-axis, respectively. The axial rotation and muscle activation are fixed for every two-dimensional map. For real-time visualization purposes, the 2D map is updated if axial rotation of muscle activation is changed, as shown in Figure 3.

B. Muscle Activation Estimation

A fundamental estimate used by our strain calculation is the muscle activation level required during shoulder movements. Due to the redundancy in muscle elements compared to the DoFs of the model, there are infinite solutions for combinations of muscle activations for any given movement/loading condition. To determine a unique solution we turn to optimization and employ the rapid muscle redundancy (RMR) solver [27]. RMR solves for individual muscle activations that generate observed estimates of joint accelerations such that the sum of muscle effort is minimized. The model computes muscle forces that account for musculotendon passive forces, muscle activation dynamics and glenohumeral joint stability to estimate physiologically realistic muscle activations in real-time.

The solver's inputs are biomechanical joint trajectories and external forces/torques acting on the subject (e.g. at the interface between robot and subject). Muscle activations are estimated by solving a nonlinear optimization problem at each time instant t_k of the human motion, minimizing the biological muscle effort expressed as a weighted sum of squared muscle activations $\mathbf{a}_k \in \mathbb{R}^{N_m}$:

$$\min_{\boldsymbol{a}(\cdot),\mathbf{c}(\cdot)} \sum_{i=1}^{N_\text{m}} w_i a_{i,k}^2 + \sum_{j=1}^{N_\text{q}} v_j c_{j,k}^2 \tag{2a}$$

subject to

$$\boldsymbol{A}_{\text{acc},k} \begin{bmatrix} \boldsymbol{a}_k \\ \boldsymbol{c}_k \end{bmatrix} = \ddot{\boldsymbol{q}}_{\text{exp},k} - \ddot{\boldsymbol{q}}_{\text{pass},k} \quad \text{acc. matching} \tag{2b}$$

$$\boldsymbol{F}_\text{GH} = \boldsymbol{A}_{\text{F},k} \begin{bmatrix} \boldsymbol{a}_k \\ \boldsymbol{c}_k \end{bmatrix} + \boldsymbol{F}_{0,k} \in \mathcal{C} \quad \text{GH stability} \tag{2c}$$

$$\forall\ i \in N_\text{m}: \quad l_{i,k} \leq a_{i,k} \leq u_{i,k} \quad \text{activation dyn.} \tag{2d}$$

Because the model is a simplified version of reality, reserve actuators were added to the model to account for model discrepancies like muscles being slack or too stretched (as recommended in [31]) and their control levels $\boldsymbol{c}_k \in \mathbb{R}^{N_q}$ were also included in the objective function (2a). The relative weights (penalties) w_i and v_j were set to 1 and 10, respectively, to promote the engagement of the muscles over

the reserve actuators, which capture modeling errors.

Constraints are used to guide the solver towards physiologically realistic solutions. First, we ensure that the simulated joint accelerations match the experimental data ($\ddot{\boldsymbol{q}}_{\mathrm{exp},k}$), by means of a linear equality constraint (2b) where we account purely for the active muscle contribution, subtracting from $\ddot{\boldsymbol{q}}_{\mathrm{exp},k}$ the influences of gravity and passive muscle forces at the given shoulder pose, collectively lumped in $\ddot{\boldsymbol{q}}_{\mathrm{pass},k}$. Element $A_{\mathrm{acc},k}(j,i)$ of $\mathbf{A}_{\mathrm{acc},k} \in \mathbb{R}^{N_q \times (N_m+N_q)}$ represents the influence of a single activation of actuator i on the acceleration of coordinate j. Secondly, a stability constraint (2c) is enforced on the joint reaction force $\boldsymbol{F}_{\mathrm{GH}}$ at the glenohumeral joint. The direction of the $\boldsymbol{F}_{\mathrm{GH}}$ was constrained to be within a circular approximation of the glenoid fossa $\mathcal{C}$, to ensure the stability of the GH joint. The last set of constraints (2d) ensures physiological activation and deactivation rates, as muscle's force generation and relaxation are dependent on the calcium ion concentrations. The dimensionless muscle activations can range between 0 and 1, where a value of 0 indicates no contraction of the fiber (no activation), and a value of 1 represents maximum muscle contraction and thus force generation (full activation).

C. Implementation of a streaming Python-RMR solver

To facilitate the integration of the RMR solver with the proposed active strain map method and a robotic system, the original implementation of the solver in MATLAB [27] was re-implemented in Python with a few important distinctions. The solver makes use of the Sequential Least Squares Programming (SLSQP) method from the Scipy.minimize library [32]. In addition, the Python implementation accommodates real-time applications by allowing for streaming pose and external forces data, which enabled us to take measurements from the robotic manipulator and compute muscle activity at approximately 5Hz such that the strain maps can be updated during an exercise based on estimated muscle activations. We tested the Python-RMR implementation against the original to verify our muscle activation estimates.

Muscle activations estimated with the RMR solver in MATLAB and Python were compared to the experimental EMG data. The activation was averaged over the three repetitions for each task. The muscle activation estimations were compared during three motions; abduction, flexion, and shrugging for both an unloaded and 2 kg load condition. To capture differences across the dataset, mean absolute errors (MAE) were computed. The MAE values for MATLAB and Python against EMG-based activations were found to be ≤ 0.17, with most values ≤ 0.10. For the majority of the activation estimations, the errors against EMG data were the same in the MATLAB and Python implementations. The differences in MAE values between MATLAB and Python were ≤ 0.02. Figure 4 included the mean and standard deviation of muscle activations for selected muscles during a loaded flexion task. The results from the experimental EMG data and the MATLAB and Python RMR implementation demonstrate that the Python-RMR solver produces results nearly identical to the MATLAB implementation, with only minor differences. Finally, we computed the average frame processing frequency of the Python-RMR solver to be approximately 5 Hz.

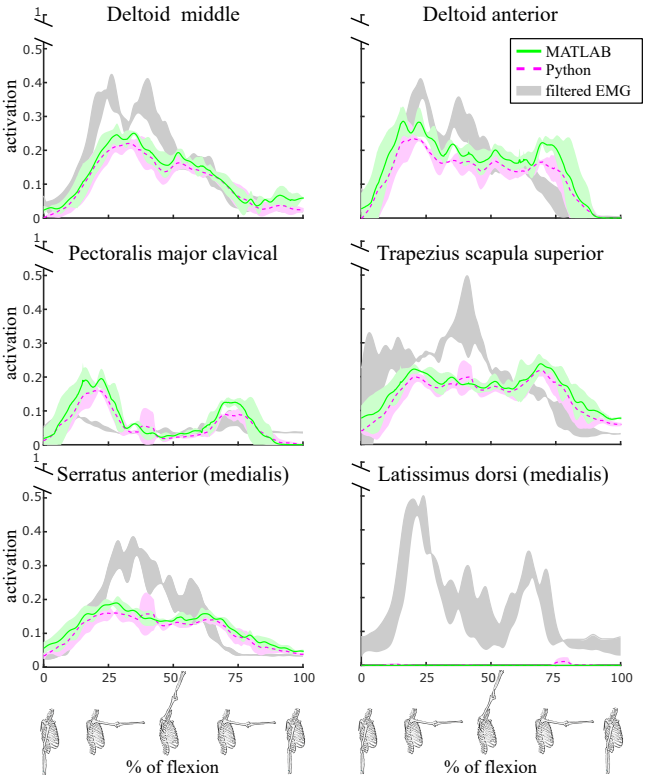

Fig. 4: Muscle activation of selected muscles during a loaded flexion motion. The estimations are shown for MATLAB (green) and Python (pink) and are displayed as the mean over three repetitions of the motion (bold lines), with a shaded ± 1 SD. Additionally, the muscle activations from filtered experimental EMG data are displayed in gray (± 1 SD).

D. Robotic Control and Interaction

The strain maps need input about the shoulder state vector $\boldsymbol{x}$ and any external forces/torques acting on the subject during the therapy to retrieve the internal biomechanics of the shoulder joint. We leveraged the KUKA LBR iiwa, a 7-DoFs industrial collaborative robot certified for safe physical human-robot interaction. A 3D-printed plastic brace is used as a rigid interface between the robot and the human arm, and the subject was instructed to minimize the displacement of their shoulder during the interaction with the robot (Figure 5). In such a way, the shoulder state $\boldsymbol{x}$ and its time derivative $\dot{\boldsymbol{x}}$ can be uniquely obtained from the current pose of the robot's end-effector. The potential discomfort to the subject is reduced by leveraging gravity compensation for both the robot and the arm brace, and interaction forces at the human-robot interface are estimated from the joint torques [33]. Data from the torque sensors and the joint angles were collected at 200Hz, and subsequently used as input for the RMR solver for the muscle activation and tendon strain estimations. During our experiments, the robot was controlled with a Cartesian impedance controller:

$$\mathbf{F}_{\mathrm{imp}} = \mathbf{K}(\overline{\mathbf{x}}_{\mathrm{ee}} - \mathbf{x}_{\mathrm{ee}}) + \mathbf{D}(\dot{\overline{\mathbf{x}}}_{\mathrm{ee}} - \dot{\mathbf{x}}_{\mathrm{ee}}) \ . \tag{3}$$

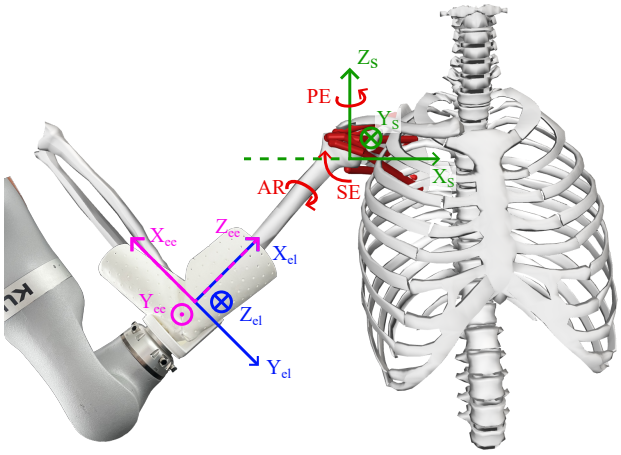

Fig. 5: An overview of the coordinate systems of the setup: The shoulder frame has its origin in the center of the glenohumeral joint (green). The glenohumeral joint DoFs (PE, SE, and AR) are shown in red. The elbow frame (blue) has an origin in the center of the elbow. The elbow frame origin coincides with that of the robot's end-effector frame (pink).

where $\mathbf{F}_{\text{imp}} \in \mathbb{R}^6$ is the vector of interaction forces and torques at the end-effector. The robot's end-effector reference and actual pose are $\overline{\mathbf{x}}_{\text{ee}}$ and $\mathbf{x}_{\text{ee}}$, respectively. $\mathbf{K}$, $\mathbf{D} \in \mathbb{R}^{6\times6}$ are the desired stiffness and damping matrices in Cartesian space. The positional and rotational stiffness of $\mathbf{K}$ are prescribed, and $\mathbf{D}$ is obtained using the double diagonalization design method [34]. By setting different positions of $\overline{\mathbf{x}}_{\text{ee}}$ at the beginning of the experiment, the robot mimics the effect of elastic bands during rehabilitation exercises (Figure 6).

E. Experimental setup

To test the integration of the muscle redundancy solver with the PTbot system we conducted an experiment to determine RC tendon strain during four different exercises. One healthy individual was considered as a subject for the following experiments. They were seated in a normal chair and, after the robot was moved to its initial position, wore the custom arm brace. The subject performed four different movements based on common rehabilitation exercises; forward flexion, extension, abduction, and adduction (see Figure 6). They were free to move in space but instructed to make 1-DoF movements. For forward flexion and extension, axial rotation and plane of elevation were kept at around $-90°$ and $90°$, respectively. In the case of abduction and adduction, axial rotation and plane of elevation were kept at around $0°$. To ensure the subject's safety, their movement was restricted within a limited ROM. For all cases, shoulder elevation was instructed to be limited between $30°$ and $80°$.

The Cartesian impedance controller of the robot was leveraged to mimic elastic bands commonly used in rehabilitation exercises. By increasing the positional stiffness, a larger external force acted on the elbow; thus, more effort was required from the subject to move along the trajectory. The four movements were all executed for three different positional stiffness values: $K_{pos} = 10$, 30, and 50 N/m. The rotational stiffness was kept constant throughout the experiments. The stiffness value K_{rot} was set to 50 Nm/rad.

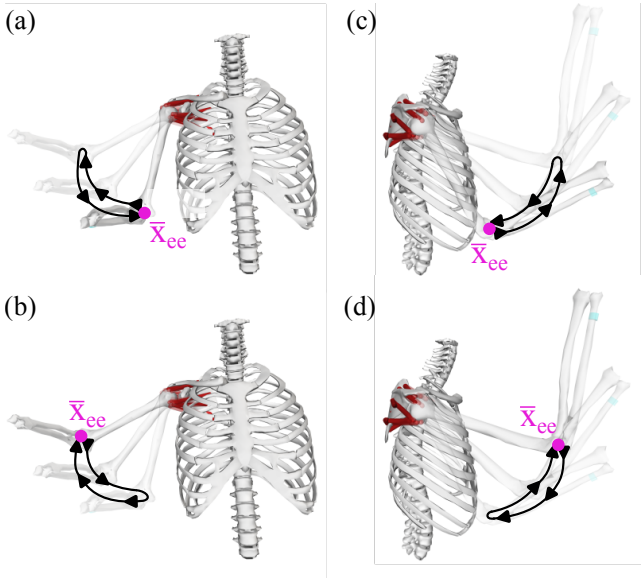

Fig. 6: The four motions as performed during the experiment with (a) abduction, (b) adduction. (c) forward flexion, (d) extension. The start position of each motion was set as the reference pose for the robot $\overline{x}_{\text{ee}}$ (pink), and the subject made one continuous motion as indicated in black. The arrows indicate the direction of the motion.

To allow for the estimation of shoulder joint angles based on the robot joint angles, the subject was instructed not to move their torso. During the experiments with the robot, we only obtained information on the GH joint coordinates and thus assumed that the scapula was not moving during the muscle activation estimation. The shoulder state and external force data were post-processed to estimate the muscle activations and the tendon strains and generate the strain maps.

All the computations were run on an HP ZBook Studio G3 with an Intel i7-6700HQ processor and 8GB RAM.

III. Results

In this section, we show the resulting muscle activations and tendon strains from the conducted experiments with a robotic device for a set of motions and show the effect of external forces on the muscle activations and, subsequently, the tendon strains (III-A). Finally, we show the resulting strain maps, which now represent active model-based tendon strain estimations during human-robot interaction in III-B.

A. Muscle activation and tendon strain estimation

The resulting muscle activation and tendon strains for the experiments performed with the Kuka LBR iiwa robotic arm are presented below. Two of the motions are shown, each with a different rotator cuff muscle highlighted. Figure 7 shows the resulting muscle activation and tendon strain of the infraspinatus inferior and infraspinatus superior during extension. A single extension was performed for three different robot stiffness values ($K = 10$ N/m, $K = 30$ N/m, and $K = 50$ N/m). By increasing the stiffness, the magnitude of the external force also increases. During extension, the infraspinatus superior is not activated for any of the modalities. The infraspinatus inferior is recruited less when the stiffness is increased, and the infraspinatus inferior

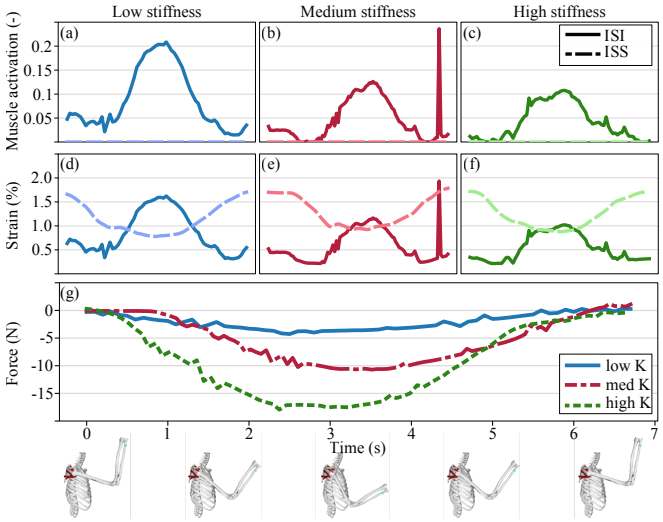

Fig. 7: An example of the shoulder extension movement and the estimated muscle strain and tendon activation of the infraspinatus inferior (ISI) and infraspinatus superior (ISS). The muscle activations (a-c) and tendon strains (d-f) are shown for all three robot stiffness values. In (g), the magnitude of the external force at the elbow is shown for the three different conditions.

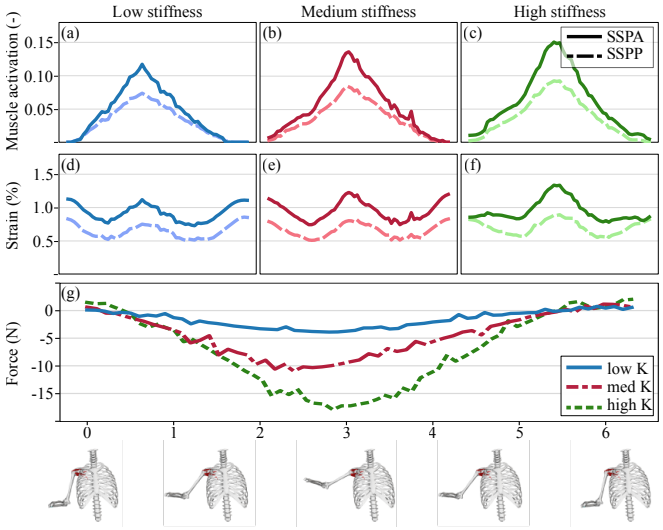

Fig. 8: An example of the shoulder abduction movement and the estimated muscle strain and tendon activation of the supraspinatus anterior (SSPA) and supraspinatus posterior (SSPP). The muscle activations (a-c) and tendon strains (d-f) are shown for all three robot stiffness values. In (g), the magnitude of the external force at the elbow is shown for the three different conditions.

tendon strain also reduces with higher stiffness. A peak at the end of the motion with medium stiffness can be seen in the infraspinatus inferior muscle activation and tendon strain. The supraspinatus muscle bundles are highlighted during a single abduction motion, again for all three stiffness values (Figure 8). Both the supraspinatus anterior and posterior bundles were activated during the abduction task. The estimated muscle activation increased with a higher positional stiffness of the robot, which also resulted in a higher tendon strain.

B. Strain maps during active rotator cuff rehabilitation

Using strain maps, we visualized the tendon strains during a single abduction motion with medium positional robot

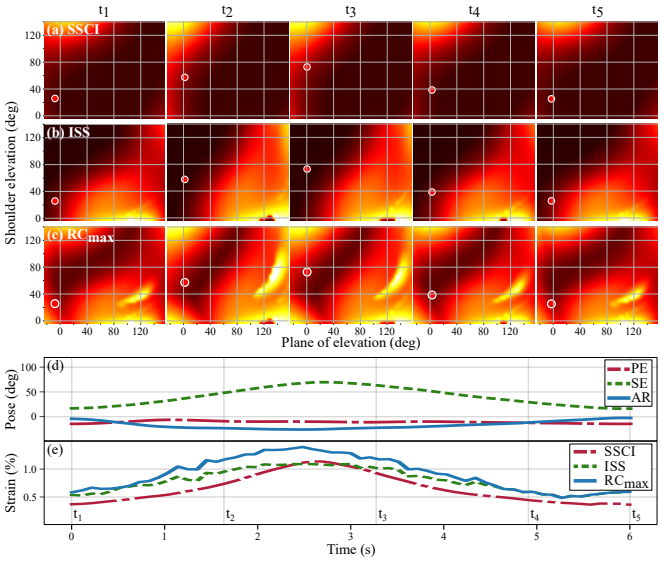

Fig. 9: An example of strain maps visualizing tendon strain at five instances ($t_1 - t_5$) during a single abduction motion with a medium stiffness (K=30 N/m). The strain maps are shown for the a) subscapularis inferior (SSCI), b) infraspinatus superior (ISS), and c) the maximum strain of all rotator cuff muscles. For the complete movement, (d) the shoulder pose and e) selected rotator cuff tendon strains are shown.

stiffness. A subset of the resulting strain maps is shown in Figure 9. They represent the strain distribution for five instances in time throughout the motion. An example of strain maps is shown for subscapularis inferior (SSCI), infraspinatus superior (ISS), and the maximum strain of all rotator cuff muscles. These maps exhibit varying shapes as the shoulder pose and muscle activation levels change throughout the motion, resulting in a shift of low and high-strain zones. Notably, the two individual muscle elements experience high strains at different shoulder poses.

IV. Discussion

In this study, we developed a method for the real-time consideration of external forces during robotic shoulder physical therapy. This is a significant step beyond our previous contributions which could not account for the RC tendon strains induced due to muscle activity and instead assumed the patient was always passive during the exercises.

The inclusion of muscle activation in the tendon strain estimator provides more physiologically realistic estimates, allowing for a larger range of rehabilitation applications. This is particularly important in later stages of rehabilitation where a patient may begin to apply greater forces (resistance training), but may still be important in earlier stages if for example the patient is simply supporting the weight of their own arm. In general, the stabilizing role of the RC muscles makes their activation (and thus the tendon strains) quite difficult to predict. Providing accurate estimates of how the activations and strains will be induced, even during fully assisted motions, is a critical step for safe robotic assistance during rehabilitation.

To prevent injury and improve rehabilitation outcomes, it is critical for a robotic PT to understand how a patient should or should not move during rehabilitation. In the case of RC

injuries, this requires insight into the RC muscle recruitment patterns and the impact these have on RC strains. The active strain maps presented here are unique in their ability to make these estimates in real-time and offer opportunities to develop new novel rehabilitation exercises tailored to the patient. In the simplest case of early-stage rehabilitation (where avoiding re-tear following surgery is crucial), a physiotherapist can choose the robot's stiffness and trajectory such that the strains in the damaged muscles are below a certain threshold. For example, in the case of an injured infraspinatus, a higher stiffness during extension was observed to reduce the strains. Conversely, during the later stages of rehabilitation, a physiotherapist may desire to prioritize strengthening a specific muscle or recruit compensatory muscles to compensate for an injured one. The combination of a customizable robotic device and the solver presents an intriguing opportunity to design and evaluate novel rehabilitation exercises for various rotator cuff disorders. This approach allows for exploring and establishing tailored rehabilitation protocols, providing valuable insights for improving patient recovery and outcomes.

The addition of muscle activation also adds substantial complexity to the strain mapping problem. While passive strain maps can be fully known beforehand, active maps rely on external forces applied by the patient which are largely unpredictable. Real-time map updates based on these external forces are thus required to correctly reflect the tendon strains during active exercises. It is thus uncertain how the strain space will evolve in each subsequent time step. For clinical implementation, further investigation is required to enable real-time updates of active strain maps while incorporating the previously identified safe and unsafe strain zones [26]. We expect to leverage tools such as model predictive control in future studies as we incorporate this complexity into our PTbot system. Additionally, the 5 Hz update speed of the Python-RMR solver is fast enough for the speed of most rehabilitation exercises, since human movement frequencies are typically within the range of 0 to 10 Hz [35]. We will improve this in the future via dedicated hardware and software.

Finally, although the object of this work is focused on robotic rehabilitation, the results also demonstrate the potential for this system to provide important insights to a human PT during physical therapy exercises. In the shoulder extension experiment for example, we observed a decreased engagement of the infraspinatus inferior as a response to the larger external forces applied to the subject (Figure 7). Notably, the tendon strains are highly dependent on changes in shoulder pose even under low muscle activity, as observed in the infraspinatus superior.

An opposing muscle response to external forces was observed in Figure 8, where the supraspinatus superior and supraspinatus inferior were activated more for higher forces. While the rotator cuff muscles are the primary stabilizers of the glenohumeral joint they also assist in the motions of the shoulder joint. The recruitment shown in Figure 8 of the supraspinatus during abduction aligns with our intuition around shoulder biomechanics for the changing external forces. Because the supraspinatus assists the deltoids in abduction, increased recruitment of both muscles was expected for increased antagonistic external forces. This recruitment can be seen clearly in Figure 8 in response to the increased stiffness of the robot.

The infraspinatus is known as the primary external rotator of the humeral head, so engagement during the extension motion, with a 90° external rotation of the humerus, is in line with these expectations. In contrast, we expected larger external forces to destabilize the glenohumeral joint and, thus, a higher engagement of the rotator cuff muscles, which was not the case for the infraspinatus inferior during extension. This may be explained by an observed increase in latissimus dorsi muscle activation, which helps depress the humerus inside the glenohumeral joint, and requires less stabilizing efforts from the infraspinatus.

These observations demonstrate the ability of this system to provide improved understanding not merely for our PTbot but clear and useful insights for physical therapists as we begin to link musculoskeletal modeling with real-time sensing and control.

V. Conclusion

In this work, we developed active strain maps, a novel functional representation of rotator cuff tendon strains in response to pose, movements and external forces on the arm. These active maps are a significant step forward from our earlier passive strain maps as they offer the ability to improve the accuracy of estimated RC tendon strains by considering the effect of muscle activation during motions and under load. We demonstrate the use of these active strain maps via our robotic physical therapy system PTbot – conducting four conventional RC therapy exercises under varying loading conditions. By connecting this active strain map framework with our PTbot system we can provide physiotherapists with safe and unsafe ROM during rehabilitation, and the ability to visualize quantitative information on tendon strain during assisted or unassisted and even resisted exercises. These active maps can be generated for every muscle element separately or can be used to represent the maximum strain experienced by all the rotator cuff muscles. Using this tool we expect to enable improved robotic perception of the RC tendon strains during robotic rehabilitation for use in the planning of custom exercises and for protecting patients during motions. Finally, strain maps paired with our PTbot system provide a novel and useful feedback tool for assisting human physiotherapists, who can receive real-time visual feedback of RC tendon strain during rehabilitation exercises and can thus leverage the different active strain maps and robot control settings to deliver therapy for specific injuries over a large ROM while reducing the risk re-injury.

References

[1] M. Urwin, D. Symmons, T. Allison, T. Brammah, H. Busby, M. Roxby, A. Simmons, and G. Williams, "Estimating the burden of musculoskeletal disorders in the community: the comparative prevalence of symptoms at different anatomical sites, and the relation to social deprivation," *Annals of the Rheumatic Diseases*, vol. 57, no. 11, pp. 649–655, 1998.

[2] M. Khan and J. J. P. Warner, "Cochrane in CORR ®: Manual therapy and exercise for rotator cuff disease," *Clin. Orthop. Relat. Res.*, vol. 475, no. 7, pp. 1779–1785, Jul. 2017.

[3] B. Mazuquin, M. Moffatt, P. Gill, J. Selfe, J. Rees, S. Drew, and C. Littlewood, "Effectiveness of early versus delayed rehabilitation following rotator cuff repair: Systematic review and meta-analyses," *PLoS One*, vol. 16, no. 5, p. e0252137, May 2021.

[4] H. Minagawa, N. Yamamoto, H. Abe, M. Fukuda, N. Seki, K. Kikuchi, H. Kijima, and E. Itoi, "Prevalence of symptomatic and asymptomatic rotator cuff tears in the general population: From mass-screening in one village," *J. Orthop.*, vol. 10, no. 1, pp. 8–12, Feb. 2013.

[5] C. Milgrom, M. Schaffler, S. Gilbert, and M. van Holsbeeck, "Rotator-cuff changes in asymptomatic adults. the effect of age, hand dominance and gender," *J. Bone Joint Surg. Br.*, vol. 77, no. 2, pp. 296–298, Mar. 1995.

[6] F. Jobe, R. Kvitne, and C. Giangarra, "Shoulder pain in the overhand or throwing athlete. the relationship of anterior instability and rotator cuff impingement," *Orthopaedic review*, vol. 18, no. 9, p. 963—975, Sep. 1989.

[7] G. K. Singh, S. Srivastava, M. Kumar, and S. Ratnakar, "Effects of selected rehabilitative exercises on external rotator muscles and trapezius muscles of masonry workers," *Work*, vol. 60, no. 3, pp. 437–444, 2018.

[8] S. T. Seroyer, S. J. Nho, B. R. Bach, Jr, C. A. Bush-Joseph, G. P. Nicholson, and A. A. Romeo, "Shoulder pain in the overhead throwing athlete," *Sports Health*, vol. 1, no. 2, pp. 108–120, Mar. 2009.

[9] U. G. Longo, A. Berton, L. Risi Ambrogioni, D. Lo Presti, A. Carnevale, V. Candela, G. Stelitano, E. Schena, A. Nazarian, and V. Denaro, "Cost-effectiveness of supervised versus unsupervised rehabilitation for rotator-cuff repair: Systematic review and meta-analysis," *Int. J. Environ. Res. Public Health*, vol. 17, no. 8, p. 2852, Apr. 2020.

[10] C. Littlewood, P. Malliaras, and K. Chance-Larsen, "Therapeutic exercise for rotator cuff tendinopathy: a systematic review of contextual factors and prescription parameters," *Int. J. Rehabil. Res.*, vol. 38, no. 2, pp. 95–106, Jun. 2015.

[11] J. Kukkonen, A. Joukainen, J. Lehtinen, K. T. Mattila, E. K. J. Tuominen, T. Kauko, and V. Aärimaa, "Treatment of non-traumatic rotator cuff tears: A randomised controlled trial with one-year clinical results," *Bone Joint J.*, vol. 96-B, no. 1, pp. 75–81, Jan. 2014.

[12] P. C. Lastayo, T. Wright, R. Jaffe, and J. Hartzel, "Continuous passive motion after repair of the rotator cuff. a prospective outcome study," *J. Bone Joint Surg. Am.*, vol. 80, no. 7, pp. 1002–1011, Jul. 1998.

[13] T. Proietti, V. Crocher, A. Roby-Brami, and N. Jarrasse, "Upper-limb robotic exoskeletons for neurorehabilitation: a review on control strategies," *IEEE reviews in biomedical engineering*, vol. 9, pp. 4–14, 2016.

[14] B. Østerås, H. Østerås, T. A. Torstensen, and O. Vasseljen, "Dose-response effects of medical exercise therapy in patients with patellofemoral pain syndrome: a randomised controlled clinical trial," *Physiotherapy*, vol. 99, no. 2, pp. 126–131, Jun. 2013.

[15] U. G. Longo, L. R. Ambrogioni, A. Berton, V. Candela, F. Migliorini, A. Carnevale, E. Schena, A. Nazarian, J. DeAngelis, and V. Denaro, "Conservative versus accelerated rehabilitation after rotator cuff repair: a systematic review and meta-analysis," *BMC Musculoskeletal Disorders*, vol. 22, no. 1, Jul. 2021. [Online]. Available: https://doi.org/10.1186/s12891-021-04397-0

[16] G. Prange, M. Jannink, C. Groothuis-Oudshoorn, H. Hermens, and M. IJzerman, "Systematic review of the effect of robot-aided therapy on recovery of the hemiparetic arm after stroke," *Journal of rehabilitation research and development*, vol. 43, pp. 171–84, 03 2006.

[17] K. Yamaguchi, A. Tetro, O. Blam, B. A. Evanoff, S. A. Teefey, and W. D. Middleton, "Natural history of asymptomatic rotator cuff tears: A longitudinal analysis of asymptomatic tears detected sonographically," *Journal of Shoulder and Elbow Surgery*, vol. 10, no. 3, pp. 199–203, 2001.

[18] A. S. Niyetkaliyev, S. Hussain, M. H. Ghayesh, and G. Alici, "Review on design and control aspects of robotic shoulder rehabilitation orthoses," *IEEE Transactions on Human-Machine Systems*, vol. 47, no. 6, pp. 1134–1145, 2017.

[19] L. Marchal-Crespo and D. J. Reinkensmeyer, "Review of control strategies for robotic movement training after neurologic injury," *Journal of neuroengineering and rehabilitation*, vol. 6, no. 1, p. 20, 2009.

[20] S. Dalla Gasperina, L. Roveda, A. Pedrocchi, F. Braghin, and M. Gandolla, "Review on patient-cooperative control strategies for upper-limb rehabilitation exoskeletons," *Frontiers in Robotics and AI*, vol. 8, p. 745018, 2021.

[21] R. Fareh, A. Elsabe, M. Baziyad, T. Kawser, B. Brahmi, and M. H. Rahman, "Will your next therapist be a robot?—a review of the advancements in robotic upper extremity rehabilitation," *Sensors*, vol. 23, no. 11, p. 5054, 2023.

[22] S. Buccelli, F. Tessari, F. Fanin, L. De Guglielmo, G. Capitta, C. Piezzo, A. Bruschi, F. Van Son, S. Scarpetta, A. Succi *et al.*, "A gravity-compensated upper-limb exoskeleton for functional rehabilitation of the shoulder complex," *Applied Sciences*, vol. 12, no. 7, p. 3364, 2022.

[23] M. Tröbinger, A. Costinescu, H. Xing, J. Elsner, T. Hu, A. Naceri, L. Figueredo, E. Jensen, D. Burschka, and S. Haddadin, "A dual doctor-patient twin paradigm for transparent remote examination, diagnosis, and rehabilitation," in *2021 IEEE/RSJ International Conference on Intelligent Robots and Systems (IROS)*. IEEE, 2021, pp. 2933–2940.

[24] S. Masiero, A. Celia, G. Rosati, and M. Armani, "Robotic-assisted rehabilitation of the upper limb after acute stroke," *Archives of Physical Medicine and Rehabilitation*, vol. 88, no. 2, pp. 142–149, 2007.

[25] J. M. Prendergast, S. Balvert, T. Driessen, A. Seth, and L. Peternel, "Biomechanics aware collaborative robot system for delivery of safe physical therapy in shoulder rehabilitation," *IEEE Robotics and Automation Letters*, vol. 6, no. 4, pp. 7177–7184, 2021.

[26] S. Balvert, J. M. Prendergast, I. Belli, A. Seth, and L. Peternel, "Enabling patient-and teleoperator-led robotic physiotherapy via strain map segmentation and shared-authority," in *2022 IEEE-RAS 21st International Conference on Humanoid Robots (Humanoids)*. IEEE, 2022, pp. 246–253.

[27] I. Belli, S. Joshi, J. M. Prendergast, I. Beck, C. D. Santina, L. Peternel, and A. Seth, "Does enforcing glenohumeral joint stability matter? a new rapid muscle redundancy solver highlights the importance of non-superficial shoulder muscles," *bioRxiv*, 2023. [Online]. Available: https://www.biorxiv.org/content/early/2023/07/12/2023.07.11.548542

[28] A. Seth, R. Matias, A. P. Veloso, and S. L. Delp, "A biomechanical model of the scapulothoracic joint to accurately capture scapular kinematics during shoulder movements," *PloS one*, vol. 11, no. 1, p. e0141028, 2016.

[29] S. L. Delp, F. C. Anderson, A. S. Arnold, P. Loan, A. Habib, C. T. John, E. Guendelman, and D. G. Thelen, "Opensim: open-source software to create and analyze dynamic simulations of movement," *IEEE transactions on biomedical engineering*, vol. 54, no. 11, pp. 1940–1950, 2007.

[30] A. Seth, R. Matias, A. P. Veloso, and S. L. Delp, "A biomechanical model of the scapulothoracic joint to accurately capture scapular kinematics during shoulder movements," *PloS one*, vol. 11, no. 1, p. e0141028, 2016.

[31] J. L. Hicks, T. K. Uchida, A. Seth, A. Rajagopal, and S. L. Delp, "Is my model good enough? best practices for verification and validation of musculoskeletal models and simulations of movement," *Journal of biomechanical engineering*, vol. 137, no. 2, 2015.

[32] P. Virtanen, R. Gommers, T. E. Oliphant, M. Haberland, T. Reddy, D. Cournapeau, E. Burovski, P. Peterson, W. Weckesser, J. Bright, S. J. van der Walt, M. Brett, J. Wilson, K. J. Millman, N. Mayorov, A. R. J. Nelson, E. Jones, R. Kern, E. Larson, C. J. Carey, İ. Polat, Y. Feng, E. W. Moore, J. VanderPlas, D. Laxalde, J. Perktold, R. Cimrman, I. Henriksen, E. A. Quintero, C. R. Harris, A. M. Archibald, A. H. Ribeiro, F. Pedregosa, P. van Mulbregt, and SciPy 1.0 Contributors, "SciPy 1.0: Fundamental Algorithms for Scientific Computing in Python," *Nature Methods*, vol. 17, pp. 261–272, 2020.

[33] A. De Luca, A. Albu-Schaffer, S. Haddadin, and G. Hirzinger, "Collision detection and safe reaction with the dlr-iii lightweight manipulator arm," in *2006 IEEE/RSJ International Conference on Intelligent Robots and Systems*. IEEE, 2006, pp. 1623–1630.

[34] A. Albu-Schaffer, C. Ott, U. Frese, and G. Hirzinger, "Cartesian impedance control of redundant robots: Recent results with the DLR-light-weight-arms," in *2003 IEEE International Conference on Robotics and Automation*, vol. 3, 2003, pp. 3704–3709.

[35] D. A. Winter, *Biomechanics and motor control of human movement*, 4th ed. Chichester, England: John Wiley & Sons, Sep. 2009.